Sescu *Advances in Difference Equations* (2015) 2015:9
DOI 10.1186/s13662-014-0343-0

Advances in Difference Equations
a SpringerOpen Journal

REVIEW Open Access

Numerical anisotropy in finite differencing

Adrian Sescu*

*Correspondence:
sescu@ae.msstate.edu
Department of Aerospace Engineering, Mississippi State University, 330 Walker at Hardy Rd, Starkville, MS 39762, USA

Abstract

Numerical solutions to hyperbolic partial differential equations, involving wave propagations in one direction, are subject to several specific errors, such as numerical dispersion, dissipation or aliasing. In the multi-dimensional case, where the waves propagate in all directions, there is an additional specific error resulting from the discretization of spatial derivatives along the grid lines. Specifically, waves or wave packets in the multi-dimensional case propagate at different phase or group velocities, respectively, along different directions. A commonly used term for the aforementioned multi-dimensional discretization error is the numerical anisotropy or isotropy error. In this review, the numerical anisotropy is briefly described in the context of the wave equation in the multi-dimensional case. Then several important studies that were focused on optimizations of finite difference schemes with the objective of reducing the numerical anisotropy are discussed.

1 Introduction

Numerical anisotropy is a discretization error that is specific to numerical approximations of multidimensional hyperbolic partial differential equations (PDE). This error is often neglected, and the focus is directed toward the reduction of other types of discretization errors, such as numerical dissipation, dispersion or aliasing (*e.g.*, Lele [1], Tam and Webb [2], Kim and Lee [3], Zingg and Lomax [4], Mahesh [5], Hixon [6], Ashcroft and Zhang [7], Fauconnier *et al.* [8] or Laizet and Lamballais [9]), or toward improving the accuracy of various time marching schemes (*e.g.*, Hu *et al.* [10], Stanescu and Habashi [11], Mead and Renaut [12], Bogey and Bailly [13] or Berland *et al.* [14]). There are several areas, however, where the numerical anisotropy can significantly affect the numerical solution based on finite difference or finite volume schemes (examples include computational acoustics, computational electromagnetics, elasticity or seismology). The numerical anisotropy can be reduced by using, for example, one-dimensional high-resolution discretization schemes, multi-dimensional optimized difference schemes, or sufficiently fine grids. However, by increasing the number of grid points the computational time may increase considerably, while one-dimensional high-resolution difference schemes may generate spurious waves at the boundaries of the domain. Oftentimes, optimizations of multi-dimensional difference schemes are more effective.

High-order finite difference schemes that are optimized in one dimension may not preserve their wave number resolution in multi-dimensional problems. These schemes may experience numerical anisotropy, because the dispersion characteristics along grid lines may not be the same as the dispersion characteristics associated with the diagonal directions. Over the years, several attempts to reduce the numerical anisotropy by vari-

ous techniques were reported. A comprehensive analysis of the numerical anisotropy was performed in the book of Vichnevetsky and Bowles [15] where, among others, the two-dimensional wave equation was solved using two different finite difference schemes for the Laplacian operator. A considerable reduction of the numerical anisotropy was attained by weight averaging the two schemes. A slightly similar approach was previously used by Trefethen [16] who used the leap frog scheme to solve the wave equation in two dimensions. Zingg and Lomax [17] performed optimizations of finite difference schemes applied to regular triangular grids that give six neighbor points for a given node. They conducted comparisons between the newly derived schemes and conventional schemes that were discretized on square grids, and found that the numerical anisotropy can be significantly reduced by using triangular grids. Tam and Webb [18] proposed an anisotropy correction to the finite difference representation of the Helmholtz equation. They derived an anisotropy correction factor using asymptotic solutions to the continuous equation and its finite difference approximation.

Jo *et al.* [19], in the context of solving the acoustic wave equation, proposed a finite difference scheme over a stencil consisting of grid points from more than one direction, by linearly combining two discretizations of the second derivative operator. A notable reduction of the numerical anisotropy was obtained, but the numerical dispersion error was increased. Hustesdt *et al.* [20] proposed a two-staggered-grid finite difference schemes for the acoustic wave propagation in two dimensions, where the first derivative operator was discretized along the grid line and along the diagonal direction. Lin *et al.* [21] explored the dispersion-relation-preserving concept of Tam and Webb [2] in two dimensions to optimize the first-order spatial derivative terms of a model equation that resembles the incompressible Navier-Stokes momentum equation. They approximated the derivative using a nine-point grid stencil, resulting in nine unknown coefficients. Eight of them were determined by employing Taylor series expansions, while the ninth one was determined by requiring that the two-dimensional numerical dispersion relation is the same as the exact dispersion relation.

Kumar [22] derived isotropic finite difference schemes for the first and second derivatives in the context of symmetric dendritic solidification, and obtained a notable reduction of the numerical anisotropy. Patra and Karttunen [23] introduced several finite difference stencils for the Laplacian, Bilaplacian, and gradient of Laplacian, with the objective of improving the isotropic characteristics. Their stencils consisted of more grid points than the conventional schemes, but it was shown that the computational cost may decrease with more than 20% due to some gain in terms of stability. Stegeman *et al.* [24] applied spectral analysis to evaluate the error in numerical group velocity (both the magnitude and the direction) of vorticity, entropy, and acoustic waves, using the numerical solution to the linearized Euler equations in two dimensions. They showed that a different measure of the group velocity error must be used to account for the error in the propagation direction of the waves. They also stressed that the numerical group velocity is more important than the numerical phase velocity in analyzing the errors associated with wave propagation. In a series of papers [25–28], Sescu *et al.* proposed a technique to derive finite difference schemes in the multi-dimensional case with improved isotropy. The optimization performed in [25–28] improved the isotropy of the wave propagation and, moreover, the stability restrictions of the multi-dimensional schemes in combination with either Runge-Kutta or linear multistep time marching methods were found to be more effective. They found that

the stability restrictions are more favorable when using multi-dimensional schemes, even if they involve more grid points in the stencils. However, this was advantageous for low order schemes, such as those of second or fourth order of accuracy, but it was also shown that favorable stability restrictions can be obtained for higher order of accuracy schemes (sixth or eight) by increasing the isotropy corrector factor. The approach was extended to prefactored compact schemes by Sescu and Hixon [29, 30]. Beside reducing the numerical anisotropy, the new multi-dimensional compact schemes are computationally cheaper than the corresponding explicit multi-dimensional scheme defined on the same stencil.

In computational electromagnetics, there were many attempts to reduce the numerical anisotropy, by applying various techniques. Berini and Wu [31] conducted a comprehensive analysis of the numerical dispersion and numerical anisotropy of finite difference schemes applied to transmission-line modeling (TLM) meshes. They found that, under certain circumstances, the time domain nodes introduce anisotropy into the dispersion characteristics of isotropic media, stressing the importance of developing schemes with improved isotropy. Gaitonde and Shang [32] proposed a class of high-order compact difference-based finite-volume schemes that minimizes the dispersion and isotropy error functions for the range of wave numbers of interest. Sun and Trueman [33] proposed an optimization of two-dimensional finite difference schemes, by considering additional nodes surrounding the point of differencing. They obtained a significant reduction in the numerical anisotropy, dispersion error and the accumulated phase errors over a broad bandwidth. Further optimizations of this scheme were performed in another paper of Sun and Trueman [34]. Koh *et al.* [35] derived a two-dimensional finite-difference time-domain method, discretizing the Maxwell equations, to eliminate the numerical dispersion and anisotropy. They showed that the new algorithm has isotropic dispersion and resembles the exact phase velocity, whose isotropic property is superior to that of other existing schemes. Shen and Cangellaris [36] introduced a new stencil for the spatial discretization of Maxwell's equations. Compared to conventional second-order accurate FDTD scheme, their scheme experienced superior isotropy characteristics of the numerical phase velocity. They also showed that the Courant number cab be increased by using the newly derived schemes. Kim *et al.* [37] derived new three-dimensional isotropic dispersion-finite-difference time-domain schemes (ID-FDTD) based on a linear combination of the traditional central difference equation and a new difference equation using extra sampling points. Among all versions of the proposed finite-difference schemes, three of them showed improved isotropy of the wave propagation compared to the original scheme of the Yee [38]. Kong and Chu [39] introduced a new unconditionally stable finite-difference time-domain method with low numerical anisotropy in three dimensions. Compared with other finite-difference time-domain methods, the normalized numerical phase velocity of their proposed scheme was significantly improved, while the dispersion error and numerical anisotropy have been reduced.

This review will describe and discuss the numerical anisotropy in the framework of wave equation and will present some of the most important optimizations of finite difference schemes in the context of reducing the numerical anisotropy. In Section 2, the dispersion error and the numerical anisotropy existing in finite difference discretizations of the wave equation are introduced and discussed. In Section 3, several approaches to reduce the numerical anisotropy, which were developed over the years by various research groups, are reviewed and discussed. Concluding remarks are included in Section 4.

2 Dispersion error and numerical anisotropy

Let us consider the centered finite difference approximation of the spatial derivative, which contains both the explicit and the implicit (or compact) parts:

$$\sum_{k=1}^{N_c} \alpha_k \left(u'_{j+k} + u'_{j-k}\right) + u'_j = \frac{1}{h}\left(\sum_{k=1}^{N_e} a_k (u_{j+k} - u_{j-k})\right) + O\left(h^n\right), \tag{1}$$

where the grid functions are $u_j = u(x_j)$ for $1 \le j \le N$, the derivatives are denoted by a prime, u'_j, h is the space step, and α_k and a_k are given coefficients. If $N_c = 0$ the scheme is termed explicit, while compact schemes (also known as implicit or Padé schemes), by contrast, have $N_c \neq 0$ and require the solution of a matrix equation to determine the derivatives along a grid line. Conventionally, the coefficients α_k and a_k are chosen to provide the largest possible exponent, n, in the truncation error, for a given stencil width, but in some instances some of these coefficients are determined to provide improved dispersion characteristics of the scheme. Table 1 includes some of these weights for various explicit and compact finite difference schemes: the explicit classical second order scheme (E2), the explicit classical fourth order scheme (E4), the explicit classical sixth order scheme (E6), the dispersion-relation-preserving scheme of Tam and Webb [2], the compact classical fourth order scheme (C4), the optimized tridiagonal compact scheme of Haras and Ta'asan [40] (Haras), the optimized pentadiagonal scheme of Lui and Lele [41] (Lui), and the spectral-like pentadiagonal compact scheme of Lele [1] (Lele). The prefactored compact scheme of Hixon [6, 42] is also included here in the form

$$\begin{aligned} &a u_{j+1}^{F'} + c u_{j-1}^{F'} + (1-a-c) u_j^{F'} = \frac{1}{h}\left[b u_{j+1} - (2b-1) u_j - (1-b) u_{j-1}\right], \\ &c u_{j+1}^{B'} + a u_{j-1}^{B'} + (1-a-c) u_j^{B'} = \frac{1}{h}\left[(1-b) u_{j+1} - (2b-1) u_j - b u_{j-1}\right], \end{aligned} \tag{2}$$

where F and B stand for 'forward' and 'backward', respectively (in a predictor-corrector time marching framework). For sixth order accuracy, $a = 1/2 - 1/(2\sqrt{5})$, $b = 1 - 1/(30a)$, and $c = 0$. The leading order term in the truncation error of a finite difference scheme depends on the choice of the coefficients and the $(n+1)$st derivative of the function u.

To study the wave number characteristics of finite difference schemes, consider a periodic domain in real space, $x \in [0, L]$, with N uniformly spaced points (the spatial step size is $h = L/N$). The discrete Fourier transform of u is given as $\hat{u}_m = \frac{1}{N}\sum_{j=1}^{N} u_j e^{-ik_m x_j}$ with $m = -N/2, \ldots, N/2-1$, where the wave number is $k_m = 2\pi m/L$. The mth component of the discrete Fourier transform of u' denoted $\hat{u}'_m$ is simply $ik_m \hat{u}_m$. Taking the discrete Fourier

Table 1 Weights of the selected spatial finite difference stencils

Stencil	α_1	α_2	a_1	a_2	a_3
E2	0	0	1/2	0	0
E4	0	0	2/3	−1/12	0
E6	0	0	3/4	−3/20	1/60
DRP	0	0	0.770882380	−0.166705904	0.020843142
C4	1/4	0	3/4	0	0
Haras	0.3534620	0	1.5669657/2	0.13995831/4	0
Lui	0.5381301	0.0666331	1.36757772/2	0.823428170/4	0.0185207834/6
Lele	0.5771439	0.0896406	1.3025166/2	0.99355/4	0.03750245/6

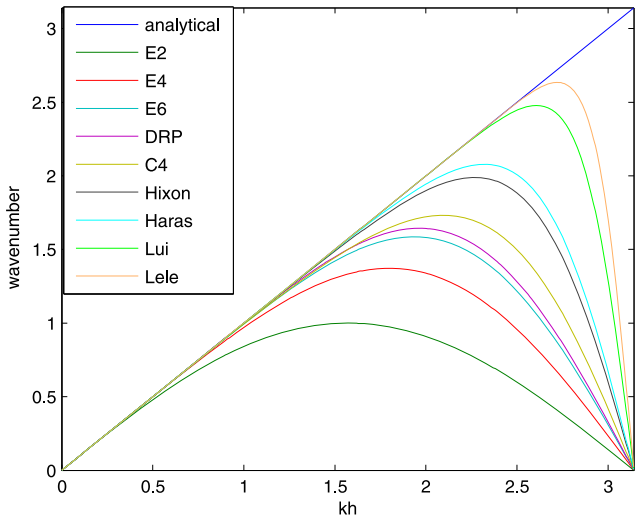

Figure 1 Numerical wave number compared to the analytical wave number.

transform of (1) implies that

$$\left(\hat{u}'_m\right)_{num} = iK(k_m h)\hat{u}_m, \tag{3}$$

where the numerical wave number is given as

$$K(z) = \frac{\sum_{n=1}^{N_e} 2a_n \sin(nz)}{1 + \sum_{n=1}^{N_c} 2\alpha_n \cos(nz)}. \tag{4}$$

Figure 1 shows the numerical wave number for various explicit and compact schemes, corresponding to those given in Table 1. The numerical wave number is compared to the analytical wave number which is represented by the straight line in Figure 1. As one can notice, the compact schemes are superior to the explicit schemes; however, compact schemes are computationally more demanding because large matrices have to be inverted.

In the multi-dimensional case, the numerical wave number and the numerical phase and group velocity are also dependent on the direction of propagation. Figure 2 shows the numerical wave number surface for the wave equation in two dimensions, corresponding to schemes E2, E6 and Hixon as given in Table 1 and (2), respectively. The cone represents the exact wave number surface, obtained by revolving the straight line from Figure 1 around the vertical axis. One can clearly notice the anisotropy in the numerical wave number surfaces associated with the finite differencing.

A simple way to reveal the numerical anisotropy is by considering the advection equation in two dimensions,

$$\partial_t u = \mathbf{c}\nabla u, \tag{5}$$

with the initial condition $u(\mathbf{r}, 0) = u_0(\mathbf{r})$, where $\mathbf{r} = (x, y)$ is the vector of spatial coordinates, $\mathbf{c} = c(\cos\alpha \sin\alpha)$ is the velocity vector (c is a scalar and α the propagation direction angle), $\nabla = (\partial_x \partial_y)^T$ and $u(\mathbf{r}, t)$ and $u_0(\mathbf{r})$ are scalar functions. A simple semi-discretization of (5)

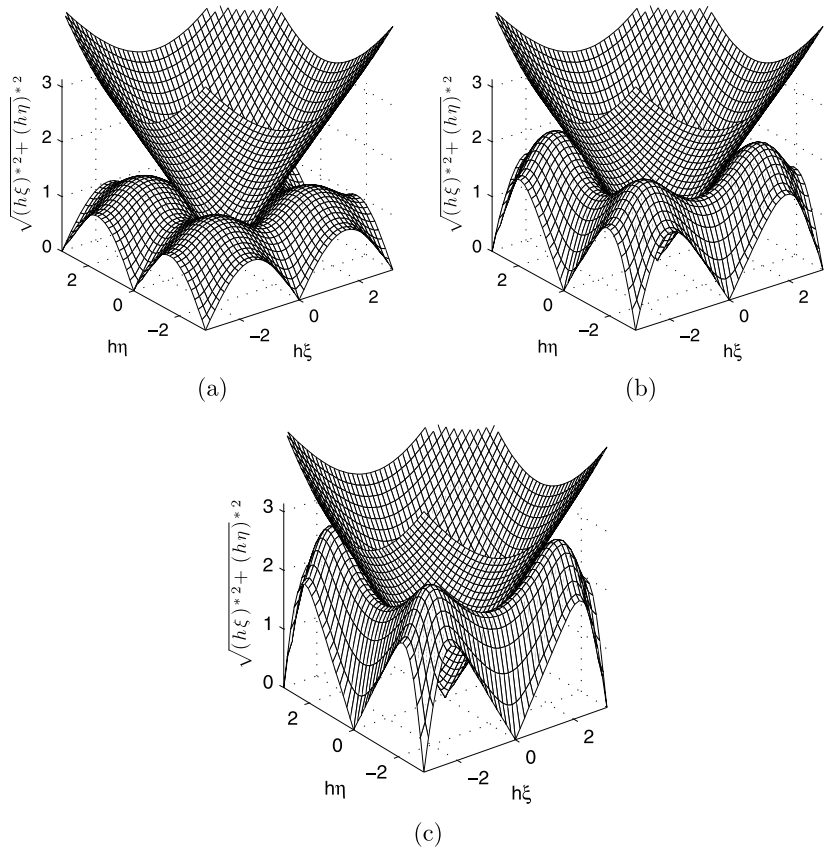

Figure 2 Numerical wave number surfaces compared to the analytical wave number surface. **(a)** Second order explicit scheme (E2); **(b)** sixth order explicit scheme (E6); **(c)** sixth order prefactored compact scheme (Hixon). The cones represent the exact wave number surfaces.

on a square grid is obtained as

$$d_t u = -\frac{c}{2h}\big[\cos\alpha(u_{i+1,j} - u_{i-1,j}) + \sin\alpha(u_{i,j+1} - u_{i,j-1})\big], \tag{6}$$

where h is the grid step. Consider the Fourier-Laplace transform:

$$\tilde{u}(\xi,\eta,\omega) = \frac{1}{(2\pi)^3}\int_0^\infty \int\int_{-\infty}^{\infty} u(x,y,t)e^{-i(\xi x+\eta y-\omega t)}\,dx\,dy\,dt, \tag{7}$$

where $\xi = K\cos\alpha$ and $\eta = K\sin\alpha$ are the components of the wave number and ω is the frequency (K is the wave number magnitude). The application of Fourier-Laplace transform to (5) gives the exact dispersion relation:

$$\omega = cK\big(\cos^2\alpha + \sin^2\alpha\big) = cK. \tag{8}$$

The exact phase velocity is given by $c_e = \omega/K = c$. By substituting ω in (7) with (8), $u(\mathbf{r},t)$ is obtained as a superposition of sinusoidal solutions in the plane with constant phase lines given by $x\cos\alpha + y\sin\alpha - c_e t = \text{const}$. As one can notice, the exact phase velocity c_e does not depend on the propagation direction α, which means that the wave propagates with

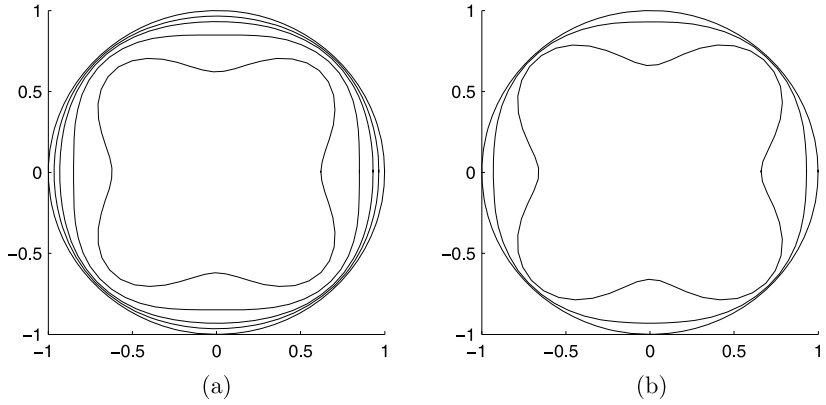

Figure 3 Polar diagram of normalized phase velocities as a function of points per wavelength (PPW) and the direction of propagation. (a) Fourth-order explicit schemes (lowest number of points per wavelength is 4); **(b)** sixth-order compact schemes (lowest number of points per wavelength is 3).

the same phase velocity in all directions (it is isotropic). Moreover, the exact group velocity defined as $g_e = \partial\omega/\partial K = c$ is the same as the exact phase velocity because the dispersion relation is a linear function of K.

We now apply the same Fourier-Laplace transform to the numerical approximation (6) and obtain the numerical dispersion relation in the form

$$\omega = \frac{c}{h}\big[\cos\alpha \sin(Kh\cos\alpha) + \sin\alpha \sin(Kh\cos\alpha)\big]. \tag{9}$$

The numerical phase velocity will be given as

$$c_n = \frac{\omega}{K} = \frac{c}{Kh}\big[\cos\alpha \sin(Kh\cos\alpha) + \sin\alpha \sin(Kh\cos\alpha)\big]. \tag{10}$$

The constant phase lines are expressed by the equation $x\cos\alpha + y\sin\alpha - c_n t = \text{const}$ and move with the phase velocity c_n. The numerical anisotropy is revealed in (10) by the dependence of the numerical phase velocity on the propagation direction angle α. In addition, the numerical group velocity is different from the numerical phase velocity (while previously, in the continuous case, they were the same),

$$g_n = \partial_K \omega = c\big[\cos^2\alpha \cos(Kh\cos\alpha) + \sin^2\alpha \cos(Kh\sin\alpha)\big], \tag{11}$$

which is also dependent on the propagation direction. This directional dependence of both phase and group velocities defines the numerical anisotropy. As an illustration, Figure 3 shows polar diagrams for two typical schemes, the fourth order explicit E4 and the sixth order compact C6 schemes, revealing the numerical anisotropy (the circle of radius 1 in Figure 3 represents the exact solution).

3 Reduction of the numerical anisotropy

In this section, several attempts to reduce the numerical anisotropy, performed by various research groups over the years, are briefly reviewed. The optimizations of the schemes are grouped according to the mathematical model: wave equation, Helmholtz equations, advection equation, Maxwell equation, and dendritic solidification equations.

3.1 Wave equation

Although the behavior of the numerical anisotropy was often reported in various one-dimensional optimizations of finite difference schemes, one of the first systematic attempts to specifically reduce the numerical anisotropy in finite difference schemes was introduced by Trefethen [16] in the framework of wave equation. To illustrate Trefethen's approach, let us consider the two-dimensional wave equation in the form

$$\partial_{tt}u = \partial_{xx}u + \partial_{yy}u, \tag{12}$$

defined in $R^2 \times [0,\infty)$, with appropriate initial and boundary conditions. Using the Fourier-Laplace transform, it is ease to find the exact dispersion relation in the form $\omega^2 = \xi^2 + \eta^2$, where ω is the frequency and (ξ,η) is the wave number vector. Equation (12) was discretized by Trefethen [16] on a Cartesian grid, using second order accurate schemes for both temporal and spatial derivatives as

$$u_{ij}^{n+1} - u_{ij}^{n} + u_{ij}^{n-1} = \frac{k^2}{h^2}\left(u_{i+1,j}^{n} + u_{i-1,j}^{n} + u_{i,j+1}^{n} + u_{i,j-1}^{n} - 4u_{i,j}^{n}\right) \tag{13}$$

which was labeled LF^2. Then the same scheme was used to discretize (12), except the spatial derivatives were approximated along the diagonal directions with the space step $\sqrt{2}h$; the latter discretization was termed LF^2. It was found that the weighted averaging $2/3LF^2 + 1/3LF_2$ provided a low numerical anisotropy in the order of $(\sqrt{\xi^2+\eta^2}h)^4$. Slightly the same approach was used by Vichnevetsky [15] who corrected the numerical isotropy of the wave propagation in two dimensions using either the linear advection equation or the wave equation.

In a series of papers, Sescu *et al.* [25–27] proposed a technique to derive explicit multi-dimensional finite difference schemes for wave equation and Euler equations. By using the transformation matrix between two orthogonal reference frames, one aligned with the grid line and the other along the diagonal direction, the multi-dimensional finite difference scheme was obtained as

$$(\partial_x u)_{i,j} = \frac{1}{h(1+\beta)}\sum_{\nu=-M}^{\nu=M} a_\nu \left(\mathbf{E}_x^\nu + \frac{\beta}{2}\mathbf{D}_x\right)\cdot u_{i,j}, \tag{14}$$

where the multi-dimensional space shift operator $\mathbf{E}_x^\nu \cdot u_{i,j} = u_{i+\nu,j}$ (see Vichnevetsky and Bowles [15] for one dimension) is used. The coefficients a_n are those from the classical centered explicit schemes. The operator $\mathbf{D}_x^\nu\cdot$ was defined as $\mathbf{D}_x^\nu\cdot = (\mathbf{E}_x^\nu\mathbf{E}_y^\nu + \mathbf{E}_x^{-\nu}\mathbf{E}_y^\nu)\cdot$ The parameter β is called isotropy corrector factor (ICF). The application of the Fourier transform to the multi-dimensional schemes gives the numerical wave number

$$(\xi h)_{\text{opt}}^{*} = \frac{2}{(1+\beta)}\sum_{n=-N}^{M} a_n\left\{e^{nI\xi h} + \frac{\beta}{2}\left[e^{nI(\xi+\eta)h} + e^{nI(\xi-\eta)h}\right]\right\}. \tag{15}$$

Then the numerical dispersion relation corresponding to two-dimensional wave equation was considered in the form $\omega^2 - [(\xi h)_{\text{opt}}^{*2} + (\eta h)_{\text{opt}}^{*2}] = 0$, and the ICF was determined by minimizing the integrated error between the phase or group velocities defined along

the x and the $x = y$ directions. Two curves in wave number-frequency space were considered: one was the intersection between the numerical dispersion relation surface and $\eta = 0$ plane, and the other was the intersection between the numerical dispersion relation surface and the $\xi = \eta$ plane. These two curves were superposed in the (Kh, ω) plane, where $Kh = [(\xi h)^2 + (\eta h)^2]^{\frac{1}{2}}$. Assuming that the equations of the two curves in (Kh, ω) plane are $\omega_1 = \omega_1(Kh, \beta)$ and $\omega_2 = \omega_2(Kh, \beta)$, the integrated error between the phase velocities was then calculated on a specified interval as $C(\beta) = \int_0^\eta |c_1(Kh, \beta) - c_2(Kh, \beta)|^2 d(Kh)$, where $c_1(Kh, \beta)$ and $c_2(Kh, \beta)$ are the numerical phase velocities. The minimization was done by equating the first derivative of $C(\beta)$ or $G(\beta)$ with zero, which provided the value of ICF, β.

Sescu *et al.* [28, 43] conducted a comprehensive stability analysis of the multi-dimensional schemes combined with either linear-multistep or multistage time marching schemes, and obtained several noteworthy results. For the Leap-Frog scheme applied to the advection equations, it was shown that the stability restriction corresponding to multi-dimensional schemes differs from the corresponding stability restriction via conventional schemes by the factor $(2\beta + 2)/(\beta + 2)$, where β is the isotropy corrector factor. The conclusion was that the stability restrictions corresponding to multi-dimensional schemes are more convenient compared to the conventional schemes. For an arbitrary direction of the convection velocity with $|c_x| \geq |c_y|$, the stability restriction for conventional stencils was given by $\sigma_x + \sigma_y \leq CFL$, where $\sigma_x = k|c_x|/h$ and $\sigma_y = k|c_y|/h$. For multi-dimensional stencils the stability restriction was given by $(1 + \beta)\sigma_x + \sigma_y \leq CFL(1 + \beta)$ (where, for example, CFL is 1, 0.72874 or 0.63052 corresponding to E2, E4 or E6 scheme, respectively). Adams-Bashforth and Runge-Kutta time marching schemes in combination with conventional and multi-dimensional schemes were also analyzed, and it was found that the multi-dimensional schemes provide less restrictive stability limits.

3.2 Helmholtz equation

Tam and Webb [18] performed an anisotropy correction of the finite difference representation of the Helmholtz equation,

$$\nabla^2 p + \xi^2 p = f, \tag{16}$$

where p is the pressure perturbation, ∇^2 is the Laplacian operator, f is the source distribution (*e.g.*, a monopole), $\xi = 2\pi/\lambda$ is the wave number, and λ is the acoustic wavelength. Tam and Webb [18] showed that the finite difference discretization of the Helmholtz equation,

$$\frac{p_{i+1,j} - 2p_{i,j} + p_{i-1,j}}{h^2} + \frac{p_{i,j+1} - 2p_{i,j} + p_{i,j-1}}{h^2} + \xi^2 p_{i,j} = f_{i,j} \tag{17}$$

with five grid points per wavelength introduces significant numerical anisotropy (equally spaced grid is assumed in both the x- and y-direction, and the spatial step is denoted as before by h). They constructed an anisotropy correction factor using asymptotic solutions to the continuous equation (16) and its finite difference approximation (17) as

$$p_a(r, \theta)_{r_{ij} \to \infty} = \left(\frac{2\pi}{\xi}\right) \frac{\pi}{ir^{1/2}} e^{i(\xi r - \pi/4)} \bar{F}\left(\bar{\alpha}_s, \bar{\beta}_+(\bar{\alpha}_s)\right) + O\left(r^{-3/2}\right) \tag{18}$$

and

$$p_n(r_{ij},\theta_{ij})_{r_{ij}\to\infty} = \frac{e^{iK_{ij}r_{ij}}}{r_{ij}^{1/2}}\left[G_0\left(\theta_{ij}+\frac{G_1(\theta_{ij}}{r_{ij}}\right)+O\left(r_{ij}^{-5/2}\right)\right], \tag{19}$$

respectively, where (r_{ij},θ_{ij}) are polar coordinates, $K_{ij}=\alpha_s(\theta_{ij})\cos\theta_{ij}+\beta_s(\theta_{ij})\sin\theta_{ij}$ (with α_s and β_s being the wave number components from the Fourier transform), and $G_0(\theta_{ij})$ and $G_1(\theta_{ij})$ are functions depending on α_s, β_s, θ, and the Fourier transform $\bar{F}$ of the source term (for more details see (19) and (21) in Tam and Webb [18]). The anisotropy corrector factor was then defined by the ratio between the absolute values of the two,

$$D(\theta,\xi h)=\frac{|p_a|}{|p_n|}. \tag{20}$$

The correction factor is independent of the distribution of sources, meaning that it can be computed once and for all types of sources. A significant reduction of the anisotropy error was obtained.

3.3 Advection equation

Gaitonde and Shang [32] proposed a class of high-order compact difference-based finite-volume schemes which minimized the dispersion and isotropy error functions for the range of wave numbers of interest. The starting point was the one-dimensional advection equation,

$$\partial_t u+\partial_x f=0,\quad f=cu, c>0 \tag{21}$$

which was discretized using a finite volume approach as

$$d_t\bar{u}_i+\bar{f}_{i+1/2}-\bar{f}_{i-1/2}=0, \tag{22}$$

where $\bar{u}$ is the average value of u inside a cell, $\bar{u}=1/h\int_{x_{i-1/2}}^{x_{i+1/2}}u\,dx$, and $\bar{f}$ is the flux function approximating f, which is dependent on the values of $\bar{u}$ from neighbor cells. The reconstruction can be done by considering a primitive function $v=\int_0^x$ which must be discretized at the cell interface. Gaitonde and Shang [32] considered a five-point compact stencil in the form

$$\alpha v_{i-1/2}+v_{i+1/2}+\alpha v_{i+3/2}=b\frac{v_{i+5/2}-v_{i-3/2}}{4h}+a\frac{v_{i+3/2}-v_{i-1/2}}{2h}, \tag{23}$$

where α, a, and b are constants which determine the order of accuracy of the scheme. Using Taylor series expansions, they sacrificed the order of accuracy of the schemes by writing a and b as functions of α,

$$a=\frac{2(2+\alpha)}{3},\qquad b=\frac{-1+4\alpha}{3} \tag{24}$$

The spectral function associated with the scheme (23) is given as

$$\hat{A}(w)=\frac{i(a\sin(w)+b\sin(2w)/2)}{1+2\alpha\cos w}, \tag{25}$$

where $w = 2\pi\xi h/L$ is the scaled wave number. The dispersion error is associated with the imaginary part of the spectral function, $w_d(w) = \mathrm{Im}(\hat{A}(w))$. A scaled isotropy wave number was defined as

$$w_i(w,\theta) = \cos(\theta) w_d\big(w\cos(\theta)\big) + \sin(\theta) w_d\big(w\sin(\theta)\big), \tag{26}$$

where θ is the angle that the direction of propagation makes with the x-axis. An isotropy error function was defined by Gaitonde and Shang [32] in the form

$$E_i(\alpha, w_{\max}) = \int_0^{w_{\max}} \int_0^{\pi/2} |w_i - w|\, d\theta dw \tag{27}$$

which was minimized to find the value of α_{opt} that gives the lowest numerical anisotropy. Numerical examples confirmed a considerable reduction of the isotropy error.

Sescu and Hixon [29, 30] extended the previous optimization performed in [26] to prefactored compact finite difference schemes [6, 42] applied to the advection equation. The prefactored compact schemes are defined on a three-point stencil and can return up to eight orders of accuracy (see equations (2)). They can be used within a predictor-corrector type time marching scheme framework (MacCormack [44]), because the numerical derivatives are determined by sweeping from one boundary to the other, in both directions. Following the same analysis as in the case of explicit schemes, the multi-dimensional prefactored compact schemes were obtained as

$$\begin{aligned} u_{i,j}^{F'} &= \frac{\alpha}{1+\beta}\left[u_{i+1,j}^{F'} + \frac{\beta}{2}\left(u_{i+1,j-1}^{F'} + u_{i+1,j+1}^{F'}\right)\right] \\ &\quad + \frac{1}{h(1+\beta)}\left[bu_{i+1,j} - eu_{i,j} + \frac{\beta}{2}(bu_{i+1,j+1} + bu_{i+1,j-1} - 2eu_{i,j})\right], \end{aligned} \tag{28}$$

$$\begin{aligned} u_{i,j}^{B'} &= \frac{\alpha}{1+\beta}\left[u_{i-1,j}^{B'} + \frac{\beta}{2}\left(u_{i-1,j-1}^{B'} + u_{i-1,j+1}^{B'}\right)\right] \\ &\quad + \frac{1}{h(1+\beta)}\left[eu_{i,j} - bu_{i-1,j} + \frac{\beta}{2}(2eu_{i,j} - bu_{i-1,j+1} - bu_{i-1,j-1})\right] \end{aligned} \tag{29}$$

for fourth order of accuracy, and

$$\begin{aligned} u_{i,j}^{F'} &= \frac{\alpha}{1+\beta}\left[u_{i+1,j}^{F'} + \frac{\beta}{2}\left(u_{i+1,j-1}^{F'} + u_{i+1,j+1}^{F'}\right)\right] \\ &\quad + \frac{1}{h(1+\beta)}\Bigg[bu_{i+1,j} - eu_{i,j} - fu_{i-1,j} \\ &\quad + \frac{\beta}{2}(bu_{i+1,j+1} - fu_{i-1,j-1} + bu_{i+1,j-1} - fu_{i-1,j+1} - 2eu_{i,j})\Bigg], \end{aligned} \tag{30}$$

$$\begin{aligned} u_{i,j}^{B'} &= \frac{\alpha}{1+\beta}\left[u_{i-1,j}^{B'} + \frac{\beta}{2}\left(u_{i-1,j-1}^{B'} + u_{i-1,j+1}^{B'}\right)\right] \\ &\quad + \frac{1}{h(1+\beta)}\Bigg[bu_{i+1,j} - eu_{i,j} - bu_{i-1,j} \\ &\quad + \frac{\beta}{2}(fu_{i+1,j+1} - bu_{i-1,j-1} + fu_{i+1,j-1} - bu_{i-1,j+1} - 2eu_{i,j})\Bigg] \end{aligned} \tag{31}$$

for sixth order of accuracy. β is the isotropy corrector factor (ICF) and its magnitude can be determined by minimizing the dispersion error corresponding to the wave-front propagating along a grid line and the wave-front propagating along a diagonal direction.

Using Fourier analysis, the numerical wave numbers and the numerical dispersion relation corresponding to the two-dimensional wave equation were found. The individual (forward or backward) numerical wave number has both real and imaginary parts: the real part of the forward operator is equal to the real part of the backward operator, and the imaginary parts are opposite. As a result, in a MacCormack predictor-corrector scheme the overall imaginary part is zero. The real parts of the numerical wave numbers corresponding to multi-dimensional schemes, for derivatives along the x-direction, were given by

$$\mathrm{Re}\big[(kh)_m^*\big] = \frac{1}{1+\beta}\left\{f_m(\eta_x) + \frac{\beta}{2}\big[f_m(\eta_x+\eta_y) + f_m(\eta_x-\eta_y)\big]\right\}, \tag{32}$$

where $m = 4$ for fourth and $m = 6$ for sixth order of accuracy, $f_4(\eta_x) = 3\sin\eta_x/(2+\cos\eta_x)$, $f_6(\eta_x) = (28\sin\eta_x + \sin 2\eta_x)/(18 + 12\cos\eta_x)$, $\eta_x = \xi h$, $\eta_y = \eta h$, and ξ and η are the components of the wave number.

In terms of numerical stability, more efficient stability restrictions were obtained as in the case of multi-dimensional explicit schemes. For example, multi-dimensional MacCormack schemes were found to provide a stability restriction in the form

$$\big[\sigma_x(1+\beta)\big]^{2/3} + \sigma_y^{2/3} \le \frac{(1+\beta)^{2/3}}{\xi_{\max}}, \tag{33}$$

if $|c_x| \ge |c_y|$, and

$$\sigma_x^{2/3} + \big[\sigma_y(1+\beta)\big]^{2/3} \le \frac{(1+\beta)^{2/3}}{\xi_{\max}}, \tag{34}$$

if $|c_y| \ge |c_x|$. For diagonal directions, with respect to the grid ($|c_x| = |c_y| = |c|$), the stability restriction becomes

$$\sigma \le \frac{(1+\beta)}{\xi_{\max}^{3/2}[1+(1+\beta)^{2/3}]^{3/2}}. \tag{35}$$

It is obvious that the right hand side of (35) is greater than $1/(2\xi_{\max})^{3/2}$ when $\beta > 0$, and it goes to $1/(\xi_{\max})^{3/2}$ when $\beta \to \infty$. This generated more efficient stability restrictions by using multi-dimensional compact schemes. Test cases showed that the multi-dimensional compact schemes were more efficient for both the fourth and the sixth order accurate schemes.

3.4 Maxwell equations

Sun and Trueman [33] performed an optimization of finite difference schemes applied to the Maxwell equations, in terms of reducing the dispersion and isotropy errors. For brevity, we show here the numerical dispersion relations (for finite differencing representations of the Maxwell equations, see (1), (2), and (4) in Sun and Trueman [33]):

$$\left(\frac{\sin(\omega k/2)}{ck}\right)^2 = \left(w\frac{\sin(\beta_a k/2)}{h} + (1-w)\frac{\sin(3\beta_a k/2)}{3h}\right)^2 \tag{36}$$

corresponding to a grid line, and

$$\left(\frac{\sin(\omega k/2)}{ck}\right)^2 = 2\left(w\frac{\sin(\beta_d k/2)}{h} + (1-w)\frac{\sin(3\beta_d k/2)}{3h}\right)^2 \tag{37}$$

corresponding to the diagonal direction, where w is a weighting factor, β_a is the numerical phase constant along the grid line, β_d is the numerical phase constant along the diagonal direction, ω is the frequency, and k is the time step (an equally spaced grid is considered again). The optimization in terms of reducing the numerical anisotropy was done by eliminating the time step terms in (36) and (37) to obtain

$$w_i = \frac{\sqrt{2}\sin(3\beta_d k/2)/(3h) - \sin(3\beta_a k/2)/(3h)}{[\sin(\beta_a k/2)/h - \sin(3\beta_a k/2)/(3h)] - \sqrt{2}[\sin(\beta_d k/2)/h - \sin(3\beta_d k/2)/(3h)]}. \tag{38}$$

This optimal weight w_i is a function of mesh density only, and is not dependent on the time step size or the frequency of the signal. This method theoretically provides a uniform phase velocity in all directions. Further optimizations of this scheme were performed in another paper of Sun and Trueman [34].

Koh *et al.* [35] derived a two-dimensional finite-difference time-domain method, discretizing the Maxwell equations, to eliminate the numerical dispersion and anisotropy. The proposed scheme is given as

$$\begin{aligned}
&d_t^2 H_{x,i,j+1/2}^n = -\frac{k}{\mu h} d_y E_{x,i,j+1/2}^n,\\
&d_t^2 H_{y,i+1/2,j}^n = -\frac{k}{\mu h} d_x E_{y,i+1/2,j}^n,\\
&d_t^2 E_{z,i,j}^{n+1/2} + \frac{\sigma k}{2\epsilon}\left[E_{z,i,j}^{n+1} + E_{z,i,j}^n\right] = \frac{k}{\epsilon h} d_x H_{y,i,j}^{n+1/2} - \frac{k}{\epsilon h} d_y H_{x,i,j}^{n+1/2},
\end{aligned} \tag{39}$$

where d_t^2 is the central difference operator with respect to time,

$$d_p f_q = \left(1 - \frac{\alpha}{2}\right) d_p f_q + \frac{\alpha}{4}\left(d_p^2 f_{q+1} + d_p^2 f_{q-1}\right) \tag{40}$$

with p or q being either x or y, and

$$d_x^2 f_{i,j} = f_{i+1/2,j} - f_{i-1/2,j}, \qquad d_y^2 f_{i,j} = f_{i,j+1/2} - f_{i,j-1/2}, \tag{41}$$

where f is a generic function. In (39), E is the electric field, H is the magnetic field strength, σ, μ, and ϵ are the conductivity, the permeability, and the permittivity, respectively, of the domain, k is the time step, and h is the spatial step in all directions. For nonconductive media, $\sigma = 0$, the numerical dispersion relation can be obtained as

$$\frac{1}{h^2} C_+ C_\times \left(\alpha - \frac{2}{C_+}\right)^2 - \frac{1}{h^2}\left(\frac{4C_\times}{C_+} - C_+\right) - \frac{1}{(ck)^2}\sin^2\left(\frac{\omega k}{2}\right), \tag{42}$$

where $C_+ = \sin^2(\xi h/2) + \sin^2(\eta h/2)$, $C_\times = \sin^2(\xi h/2)\sin^2(\eta h/2)$, and ξ and η are the components of the wave number. Equation (42) is a quadratic equation in α, and the solution

is given as

$$\alpha = \frac{2}{C_+}\left[1 - \sqrt{1 - \frac{h^2 C_+}{4C_\times}\left(\frac{1}{h^2}C_+ - \frac{1}{(ck)^2}\sin^2\left(\frac{\omega k}{2}\right)\right)}\right]. \tag{43}$$

An optimal value for α, achieving an isotropic numerical phase velocity, can be simply estimated as the mean value of α over the azimuthal angles, and it was found that it remains constant (approximately, 0.167) for a wide range of grid sizes, and it is insensitive to the value of the Courant number.

Kim *et al.* [37] derived new three-dimensional isotropic dispersion-finite-difference time-domain schemes (ID-FDTD) based on a linear combination of the traditional central difference equation and a new difference equation based on the extra sampling points. They used the same scaling factors as for the two-dimensional case to attain the isotropic dispersion and the exact phase velocity. Based on the weighting factors, seven different FDTD schemes were formulated, including the Yee scheme [38]. Among the seven proposed FDTD schemes, three showed improved isotropy of the dispersion compared to the dispersion of the Yee scheme. For the sake of brevity, the complete expressions of the schemes are not included here (see Kim *et al.* [37] for more details), and only the numerical dispersion relation is briefly presented. Plane wave solutions were introduced in discretized forms as

$$\mathbf{E}_{i,j}^{n} = \mathbf{E}_0 e^{I(n\omega k - \xi ih - \eta jh - \zeta kh)}, \tag{44}$$

$$\mathbf{H}_{i,j}^{n} = \mathbf{H}_0 e^{I(n\omega k - \xi ih - \eta jh - \zeta kh)}, \tag{45}$$

where $I = \sqrt{-1}$, ω is the frequency, (ξ, η, ζ) is the numerical wave number vector, and $\mathbf{E}_0$ and $\mathbf{H}_0$ are constant vectors. After inserting (44) and (45) into the discretized form of the Maxwell equations (see (10) in Kim *et al.* [37]), the matrix equations are obtained as $C\mathbf{H}_0 = S_t\epsilon_0\mathbf{E}_0$, $C\mathbf{E}_0 = S_i\mu_0\mathbf{H}_0$ where

$$C = \begin{bmatrix} 0 & -K_z & K_y \\ K_z & 0 & -K_x \\ -K_y & K_x & 0 \end{bmatrix} \tag{46}$$

and $K_p = S_p/h[\alpha(P_p - Q_p) - \beta Q_p/2 + 1]$ (p being either x, y or z), $S_x = \sin(\xi h/2)$, $S_y = \sin(\eta h/2)$, $S_z = \sin(\zeta h/2)$, $P_x = SySz$, $P_y = SxSz$, $P_z = SxSy$, $Q_x = S_y^2 + S_z^2$, $Q_y = S_x^2 + S_z^2$, $Q_z = S_x^2 + S_y^2$, and $S_t = \sin\omega k/2/k$. The eigenvalue equation was obtained as

$$\left(C^2 + S_t^2\mu_0\epsilon_0 I\right) = 0, \tag{47}$$

and the numerical dispersion relation was obtained by vanishing of the associated determinant,

$$\frac{S_t^2}{c_0^2} = K_x^2 + K_y^2 + K_z^2, \tag{48}$$

where $c_0 = 1/\sqrt{\epsilon_0\mu_0}$. The isotropy correction was performed by defining the values of the weighting factors α and β, which unlike the two-dimensional case are not unique. Kim

et al. [37] used the scaling factor from the two-dimensional case, and they modified the numerical dispersion relation to estimate the weighting factors.

3.5 Dendritic solidification

Kumar [22] derived isotropic finite difference schemes for the first and second derivatives in the context of symmetric dendritic solidification. The first derivative was discretized as

$$(\partial_x u)_{I,i,j} = \frac{1}{2h}\left[\frac{1}{6}(u_{i+1,j+1} - u_{i-1,j+1}) + \frac{4}{6}(u_{i+1,j} - u_{i-1,j}) + \frac{1}{6}(u_{i+1,j-1} - u_{i-1,j-1})\right], \tag{49}$$

which involves grid points not only along the x-direction, but also along the y-direction. The Taylor expansion of the scheme (49) can be written as $(\partial_x u)_{I,i,j} = (1 + h^2/6\nabla^2)(\partial_x u)_{i,j}$, where the leading order term involves the Laplacian only, implying no directional dependence. The second derivative was discretized as

$$\begin{aligned}(\partial_{xx} u)_{I,i,j} = \frac{1}{h^2}\Bigg[&\frac{1}{12}(u_{i+1,j+1} - 2u_{i,j+1}u_{i-1,j+1}) + \frac{10}{12}(u_{i+1,j} - 2u_{i,j} + u_{i-1,j}) \\ &+ \frac{1}{12}(u_{i+1,j-1} - 2u_{i,j-1} + u_{i-1,j-1})\Bigg],\end{aligned} \tag{50}$$

where the Taylor expansion is given by $(\partial_{xx} u)_{I,i,j} = (1 + h^2/12\nabla^2)(\partial_{xx} u)_{i,j}$, it being again a function of the Laplacian only. The conventional cross derivative $(\partial_{xy} u)_{I,i,j}$ was found to be intrinsically isotropic according to the criterion developed by Kumar [22]. The Laplacian can be obtained by combining the isotropic derivatives along the x- and y-directions, $(\nabla^2 u)_{i,j} = (\partial_{xx} u)_{I,i,j} + (\partial_{yy} u)_{I,i,j}$. A significant reduction of the numerical anisotropy was obtained by using these schemes. Shen and Cangellaris [36] exploited further this approach to develop new isotropic finite-difference time-domain schemes modeling electromagnetic wave propagation.

4 Concluding remarks

The numerical anisotropy in finite difference discretizations of partial differential equations was discussed and reviewed. In some instances, the numerical anisotropy can be neglected, and the focus is directed toward other types of one-dimensional errors, such as numerical dispersion, dissipation or aliasing. These errors can be analyzed in the context of one-dimensional difference equations, while the extension to multi-dimensional discretizations is straightforward. By increasing the accuracy of one-dimensional schemes or by increasing the number of grid points in the grid, the isotropic characteristics of the waves in the multi-dimensional case can be improved. These two practices, however, are not always effective since an increase in accuracy may require larger stencils which may introduce spurious waves at the boundaries of the domain, while by increasing of the resolution of the grid one may increase the computational time. It is necessary then to analyze the schemes in the multi-dimensional case and design specific optimizations with the specific objective of reducing the numerical anisotropy, and at the same time of conserving the dispersion characteristics of the corresponding one-dimensional schemes. Various attempts to reduce the numerical anisotropy in finite differencing applied to various model equations were presented and discussed.

Future directions should focus on optimizations of existing compact finite difference schemes in terms of reducing the numerical anisotropy, or derivations of novel compact schemes with low numerical anisotropy. Optimizations and derivations of finite volume schemes (in terms of reducing the numerical anisotropy) applied to either structured or unstructured grids should also be taken into account, especially in the framework of wave propagation problems. Filtering schemes, as applied, for example, in large eddy simulations to separate the small scales from the large scales, may experience numerical anisotropy since they are effective at high wave number ranges. Optimizations of such filters in terms of reducing the numerical anisotropy is also another future area of research.

Competing interests
The author declares that they have no competing interests.

Acknowledgements
The author would like to thank Ray Hixon, Abdollah Afjeh, Vasanth Allampalli, Shivaji Medida, Daniel Ingraham, and Carmen Sescu for constructive support and encouragement.

Received: 15 July 2014 Accepted: 25 December 2014 Published online: 16 January 2015

References

1. Lele, SK: Compact finite difference schemes with spectral-like resolution. J. Comput. Phys. **103**, 16-42 (1992)
2. Tam, CKW, Webb, JC: Dispersion-relation-preserving finite difference schemes for computational aeroacoustics. J. Comput. Phys. **107**, 262-281 (1993)
3. Kim, JW, Lee, DJ: Optimized compact finite difference schemes with maximum resolution. AIAA J. **34**, 887-893 (1996)
4. Zingg, DW, Lomax, H, Jurgens, HM: High-accuracy finite-difference schemes for linear wave propagation. SIAM J. Sci. Comput. **17**, 328-346 (1996)
5. Mahesh, K: A family of high order finite difference schemes with good spectral resolution. J. Comput. Phys. **145**, 332-358 (1998)
6. Hixon, R: Prefactored small-stencil compact schemes. J. Comput. Phys. **165**, 522-541 (2000)
7. Ashcroft, G, Zhang, X: Optimized prefactored compact schemes. J. Comput. Phys. **190**, 459-477 (2003)
8. Fauconnier, D, De Langhie, C, Dick, E: A family of dynamic finite difference schemes for large-eddy simulation. J. Comput. Phys. **228**, 1830-1861 (2009)
9. Laizet, S, Lamballais, E: High-order compact schemes for incompressible flows: a simple and efficient method with quasi-spectral accuracy. J. Comput. Phys. **228**, 5989-6015 (2009)
10. Hu, FQ, Hussaini, MY, Manthey, JL: Low-dissipation and low-dispersion Runge-Kutta schemes for computational acoustics. J. Comp. Physiol. **124**, 177-191 (1996)
11. Stanescu, D, Habashi, WG: 2N-storage low-dissipation dispersion Runge-Kutta schemes for computational acoustics. J. Comput. Phys. **143**, 674-681 (1998)
12. Mead, JL, Renaut, RA: Optimal Runge-Kutta methods for first order pseudospectral operators. J. Comp. Physiol. **152**, 404-419 (1999)
13. Bogey, C, Bailly, C: A family of low dispersive and low dissipative explicit schemes for flow and noise computation. J. Comp. Physiol. **194**, 194-214 (2004)
14. Berland, J, Bogey, C, Bailly, C: Low-dissipation and low-dispersion fourth-order Runge-Kutta algorithm. Comput. Fluids **35**, 1459-1463 (2006)
15. Vichnevetsky, R, Bowles, JB: Fourier Analysis of Numerical Approximations of Hyperbolic Equations. SIAM Studies in Applied Mathematics. SIAM, Philadelphia (1982)
16. Trefethen, LN: Group velocity in finite difference schemes. SIAM Rev. **24**, 113 (1982)
17. Zingg, DW, Lomax, H: Finite difference schemes on regular triangular grids. J. Comput. Phys. **108**, 306-313 (1993)
18. Tam, CKW, Webb, JC: Radiation boundary condition and anisotropy correction for finite difference solutions of the Helmholtz equation. J. Comput. Phys. **113**, 122-133 (1994)
19. Jo, CH, Shin, CS, Suh, JH: An optimal 9 point finite difference, frequency-space, 2-D wave extrapolator. Geophysics **61**, 529-537 (1996)
20. Hustesdt, B, Operto, S, Virieux, J: Mixed-grid and staggered-grid finite-difference methods for frequency-domain acoustic modeling. Geophys. J. Int. **157**, 1269-1296 (2004)
21. Lin, RK, Sheu, TWH: Application of dispersion-relation-preserving theory to develop a two-dimensional convection-diffusion scheme. J. Comput. Phys. **208**, 493-526 (2005)
22. Kumar, A: Isotropic finite-differences. J. Comput. Phys. **201**, 109-118 (2004)
23. Patra, M, Karttunen, M: Stencils with isotropic discretization error for differential operators. Numer. Methods Partial Differ. Equ. **22**, 936-953 (2006). doi:10.1002/num.20129
24. Stegeman, PC, Young, ME, Soria, J, Ooi, A: Analysis of the anisotropy of group velocity error due to spatial finite difference schemes from the solution of the 2D linear Euler equations. Int. J. Numer. Methods Fluids **71**, 805-829 (2013)
25. Sescu, A, Hixon, R, Afjeh, AA: Anisotropy Correction of Two Dimensional Finite Difference Schemes for Computational Aeroacoustics. AIAA Paper 2007-3495 (2007)
26. Sescu, A, Hixon, R, Afjeh, AA: Multidimensional optimization of finite difference schemes for computational aeroacoustics. J. Comput. Phys. **227**, 4563-4588 (2008)

27. Sescu, A, Afjeh, AA, Hixon, R: Optimized difference schemes for multidimensional hyperbolic PDEs. Electron. J. Differ. Equ. Conf. **17**, 213-225 (2009)
28. Sescu, A, Hixon, R, Sescu, C, Abdollah, AA: Stability Investigation of Multidimensional Optimized Spatial Stencils. AIAA Paper 2009-0005 (2009)
29. Sescu, A, Hixon, R: Multidimensional Prefactored Compact Schemes. AIAA Paper 2012-1175 (2012)
30. Sescu, A, Hixon, R: Numerical anisotropy study of a class of compact schemes. J. Sci. Comput. (2014). doi:10.1007/s10915-014-9826-0
31. Berini, J, Wu, K: A comprehensive study of numerical anisotropy and dispersion in 3-D TLM meshes. IEEE Trans. Microw. Theory Tech. **43**, 1173-1181 (1995)
32. Gaitonde, D, Shang, JS: Optimized compact-difference-based finite-volume schemes for linear wave phenomena. J. Comput. Phys. **138**, 617-643 (1997)
33. Sun, G, Trueman, CW: Optimized finite-difference time-domain methods based on the (2,4) stencil. IEEE Trans. Antennas Propag. **53**, 832-842 (2005)
34. Sun, G, Trueman, CW: Suppression of numerical anisotropy and dispersion with optimized finite-difference time-domain methods. IEEE Trans. Antennas Propag. **53**, 4121-4128 (2005)
35. Koh, I, Kim, H, Lee, J-M, Yook, J-G, Pil, CS: Novel explicit 2-D FDTD scheme with isotropic dispersion and enhanced stability. IEEE Trans. Antennas Propag. **54**, 3505-3510 (2006)
36. Shen, G, Cangellaris, AC: A new FDTD stencil for reduced numerical anisotropy in the computer modeling of wave phenomena. Int. J. RF Microw. Comput.-Aided Eng. **17**, 447-454 (2007)
37. Kim, W-T, Koh, I-S, Yook, J-G: 3D isotropic dispersion (ID)-FDTD algorithm: update equation and characteristics analysis. IEEE Trans. Antennas Propag. **58**, 1251-1259 (2010)
38. Yee, K: Numerical solution of initial boundary value problems involving Maxwell's equations in isotropic media. IEEE Trans. Antennas Propag. **14**, 302-307 (1966)
39. Kong, Y-D, Chu, Q-X: An unconditionally-stable FDTD method with low anisotropy in three-dimensional domains. In: Proceedings of Progress in Electromagnetics Research Symposium, Kuala Lumpur, Malaysia (2012)
40. Haras, Z, Ta'asan, S: Finite-difference schemes for long-time integration. J. Comput. Phys. **114**, 265-279 (1994)
41. Lui, C, Lele, SK: Direct Numerical Simulation of Spatially Developing, Compressible, Turbulent Mixing Layers. AIAA Paper 2001-0291 (2001)
42. Hixon, R, Turkel, E: Compact implicit MacCormack-type schemes with high accuracy. J. Comput. Phys. **158**, 51-70 (2000)
43. Sescu, A, Afjeh, AA, Hixon, R, Sescu, C: Conditionally stable multidimensional schemes for advective equations. J. Sci. Comput. **42**, 96-117 (2009)
44. MacCormack, RW: The Effect of Viscosity in Hypervelocity Impact Cratering. AIAA Paper 69-354 (1969)